

Magnetic field dependence of vortex activation energy: a comparison between MgB_2 , NbSe_2 and $\text{Bi}_2\text{Sr}_2\text{Ca}_2\text{Cu}_3\text{O}_{10}$ superconductors

S. D. Kaushik¹, V. Braccini² and S. Patnaik¹

1 School of Physical Sciences, Jawaharlal Nehru University, New Delhi 110067, India.

2 CNR-INFN LAMIA, C.so, Perrone 24, 16152, Genova, Italy

Corresponding author e-mail: spatnaik@mail.jnu.ac.in

Abstract

The dissipative mechanism at low current density is compared in three different classes of superconductors. This is achieved by measurement of resistance as a function of temperature and magnetic field in clean polycrystalline samples of NbSe_2 , MgB_2 and $\text{Bi}_2\text{Sr}_2\text{Ca}_2\text{Cu}_3\text{O}_{10}$ superconductors. Thermally activated flux flow behavior is clearly identified in bulk MgB_2 . While the activation energy at low fields for MgB_2 is comparable to $\text{Bi}_2\text{Sr}_2\text{Ca}_2\text{Cu}_3\text{O}_{10}$, its field dependence follows a parabolic behavior unlike a power law dependence seen in $\text{Bi}_2\text{Sr}_2\text{Ca}_2\text{Cu}_3\text{O}_{10}$. We analyze our results based on the Kramer's scaling for grain boundary pinning in MgB_2 and NbSe_2 .

PACS No.: 74.25.Qt, 74.70.Ad, 74.78.Db

Keywords: Vortex state, Arrhenius plot, Vortex activation energy, Resistive broadening.

Introduction

Technological applicability of superconductors depends on several parameters such as high transition temperature, high upper critical field, low anisotropy and the ability to sustain high current densities at elevated temperatures. In spite of higher transition temperature (T_c) in copper oxide based superconductors (with upper critical field in the excess of 150 Tesla), practically the entire superconducting magnet industry centers on liquid helium cooled niobium based superconductors. This is because the in-field critical current density, that is the maximum current density before the onset of dissipation at a given field, is severely suppressed in high T_c materials. Particularly disconcerting is the appearance of resistive behavior at extremely small current densities at all finite temperatures [1]. This happens because of thermally activated hopping of vortex bundles (TAFF) across the pinning sites even if the Lorentz force due to the transport current is much smaller compared to the pinning force at the defect sites. In this respect the advent of two band superconductor magnesium diboride with $T_c \sim 39$ K [2], anisotropy $\gamma \sim 3$ [3] and upper critical field $H_{c2}(0) \sim 60$ T [4] holds promise, especially in conjunction with liquid cryogen free close cycle refrigerators [5]. Similar considerations require that bulk MgB_2 must be robust against lossy transport at ~ 20 K, the base temperature of single stage cryocoolers.

The clear signature of the thermally activated vortex dynamics is the broadening of superconducting transition in the presence of external magnetic field. However this is not a sufficient condition because the broadening can also be attributed to several other reasons. It may simply be caused by inhomogeneous microstructure with different phases having different transition temperatures. This aspect can be easily verified by the transition width at zero external fields. There are some reports that suggest that the broadening can be due to surface and multiband superconductivity [6]. But in general terms, it is understood that the vulnerability to thermal fluctuations in superconductors is well characterized by the Ginzburg number (Gi) =

$(k_B T_c / H_c(0) \xi_c \xi_{ab}^2)^2 / 2$, where ξ_{ab} , ξ_c are coherence lengths for H perpendicular to ab plane and c-axis respectively. The estimated value of G_i for BSCCO is of the order of 10^{-2} whereas that for NbSe₂ is reported as low as 10^{-8} [7]. For MgB₂, Angst et al. have separately suggested a value of 10^{-5} which is in the intermediate range [8]. We choose NbSe₂ for comparison because it is a low T_c superconductor and has electronic anisotropy that is comparable to MgB₂. Recently it has also been discussed as a multigap superconductor [9]. In essence our approach is to study and compare the lossy transport in three classes of superconductors in a material form that is closest to long length cables. First we seek to answer whether thermally activated flux flow theories are applicable to polycrystalline MgB₂. While TAFF has been reported in thin films of MgB₂ [10], in this paper we clearly identify this in polycrystalline MgB₂. In spite of large variation in G_i , we observe TAFF behavior in all three superconductors. Our results show that the TAFF activation energy $U_0(T, B)$ follows a parabolic dependence with magnetic field for MgB₂ and NbSe₂ where as it exhibits power law decay in the case of the cuprate BSCCO. The parabolic dependence is interpreted as a consequence of grain boundary pinning. Further, the magnitude of activation energy at low fields is comparable in BSCCO and NbSe₂ but it is an order of magnitude higher in MgB₂.

Experiment

Polycrystalline samples of MgB₂ and NbSe₂, and highly c-axis oriented platelets of BSCCO, extracted from silver sheathed tapes, are used in the study. The preparation methods of these samples have been reported elsewhere [11, 12]. The dimension of these samples are $1 \times 3 \times 0.5 \text{ mm}^3$, $2 \times 5 \times 0.12 \text{ mm}^3$ and $2 \times 4 \times 0.2 \text{ mm}^3$ for MgB₂ bulk, BSCCO and NbSe₂, respectively. Silver sheath of BSCCO tape was removed by etching with NH₄OH and H₂O₂ solution. Linear four-probe technique was used for resistance and I-V measurement. The external field was varied

in the range from 0 - 7 T and the direction of transport probe current was kept perpendicular to the applied field. Care was taken in selecting the correct magnitude of probe current so that it followed Ohmic behavior in normal state in each case and yet did not lead to pronounced sample heating. For bulk MgB₂ and NbSe₂ current was chosen to be 20 mA, and for BSCCO it was 15 mA. All measurements were performed in warming cycle after zero field cooling. The data were taken in a “Cryogenic” 8 Tesla cryogen free magnet system with an attached variable temperature insert.

Results and discussion

Figure 1 shows the normalized resistivity as a function of reduced temperature at various applied magnetic field for MgB₂ bulk, BSCCO, and NbSe₂. The inset in each layer shows the zero field resistivity as a function of temperature and marks the superconducting transition temperature. We also note that the temperature dependence of normal state resistivity in the three samples is entirely different. For NbSe₂ the features of charge density wave at $T \sim 35$ K is clearly identified [13]. On the other hand MgB₂ shows robust metallic behavior from room temperature to 40 K. The T_c is found to be 110 K for BSCCO, 39 K for intermetallic polycrystalline MgB₂, and 7.5 K for NbSe₂. The zero field transition width for MgB₂ is ~ 0.45 K, for NbSe₂ it is ~ 0.15 K while for BSCCO it is ~ 1.5 K. The residual resistance ratio ($\rho_{(T=300K)} / \rho_{(T=T_c)}$) is estimated to be 4.3, 14.4, and 12.7 for BSCCO, MgB₂ bulk, and NbSe₂ respectively. High RRR values point towards relative clean limit of the sample. The numbers are lower than single crystal values and are attributed to the presence of grain boundary defects in polycrystalline samples. Recently Rowell et al. have defined $\rho_{300K} - \rho_{T_c}$ instead of RRR as the true parameter for determination of intergrain connectivity [14]. The values so calculated, normalized to the respective room temperature resistivity, are found to be 0.76, 0.97, and 0.92 for BSCCO, MgB₂ bulk, and NbSe₂

respectively. Therefore the bulk samples have similar intergrain connectivity and thus are suitable for comparison of vortex activation energy. We also note that all the samples in the present study show significant broadening in transition width that increases with application of magnetic field. This is most pronounced in the case of BSCCO. In high T_c BSCCO, the magneto-resistance curves near T_c merge together whereas both in MgB_2 and $NbSe_2$ bulk we observe noticeable shift of the onset with the application of field.

While there have been some reports indicating flux creep from magnetization studies in polycrystalline MgB_2 [15], it is still an open question if it has TAFF origin. By definition, TAFF is observed in a narrow window of small current density above the irreversibility line where the $\log \rho$ versus $\log E$ curve shows a linear dependence in contrast to a weak non linear behavior at higher current densities which is explained by Bardeen – Stephan Flux flow model [16]. This curvature change is the essential evidence for the TAFF model to be applicable. Shown in figure 2 is the $\log \rho$ versus $\log E$ curve for the MgB_2 bulk sample at $\mu_0 B = 3$ T. As the temperature increases, there is a clear transition from a highly nonlinear behavior below $T < T_{irr}$ (~ 28.25 K) to a regime of weakly nonlinear behavior with finite resistance above $T > T_{irr}$. The weakly nonlinear behavior has two regimes. At low currents, the resistivity is due to TAFF whereas at higher current it is due to flux flow resistivity given by $\rho_F = \rho_n B / B_{c2}$, where ρ_n is the normal state resistivity. In the TAFF regime, the resistivity is given by [1]

$$\rho_{TAFF}(T, B) = (\nu_0 \phi_0^2 L_c / k_B T) \exp(-U_0(T, B) / k_B T) = \rho_0 \exp(-U_0(T, B) / k_B T) \quad (1)$$

Here ν_0 is the attempt frequency for the hopping of flux bundles ($\sim 10^{12}$ Hz), ϕ_0 is the flux quantum (2×10^{-7} Gcm²), L_c is the length of the vortex bundle and U_0 is the vortex activation energy. In the amorphous limit, the activation energy is given as $U_0 = (J_c \times B) V_c r_p = (J_c \times B) a_0^2 L_c \xi$, where V_c is volume of the flux bundle $R_c^2 L_c$, with $R_c \sim$ intervortex distance a_0 , and $r_p \sim \xi$ that is the

range of pinning potential [1]. In figure 3 we show the Arrhenius plots of resistivity in the logarithmic scale versus inverse of temperature. A linear regime is seen in all the four samples with the most pronounced effects in BSCCO. The magnitude of activation energy U_0 is directly related to the slope of a straight line drawn on Arrhenius curves in the region of resistivity lower than 10 % of normal state resistivity. From Fig.3, the extrapolated value of ρ_0 for MgB_2 is $2.38 \times 10^3 \mu\Omega\text{-cm}$, for BSCCO it is $2.5 \times 10^3 \mu\Omega\text{-cm}$ and for $NbSe_2$ this value is $2.9 \times 10^5 \mu\Omega\text{-cm}$. These values are more than two orders of magnitude higher than the normal state resistivity value ρ_n (at T_c).

The dependence of activation energy on magnetic field has attracted considerable attention in the recent past [1]. In Figure 4 we plot the activation energy U_0 , determined from the magnetoresistance study versus applied magnetic field. Following Thompson et al.[17], we fit the data using the equation

$$U(B) = aB^\gamma(1-B/B^*)^\delta \quad (2)$$

Where B is the applied magnetic field, B^* is the irreversibility field, and a, γ, δ are scaling parameters. Here the component $(1-B/B^*)^\delta$ represents suppression of superconducting property due to the application of magnetic field and the component B^γ represents the variation due to decreasing critical current density. For $t < 0.9$ Equation 2 fits well for MgB_2 sample with the fitting parameter $\gamma = -0.39$, $\delta = 2.1$ with irreversibility field $B^* = 9.67$ T and $a = 3410$ K. The goodness of the fit $R^2 = 0.95$. On fitting U versus H curve in MgB_2 we find a clear signature of parabolic behavior. The fitting parameters and the value of U_0 is of the same order as has been calculated for MgB_2 polycrystalline thin films by Thompson and our previous report [17, 10]. Thus the activation energy in bulk sample is of the same order as compared to polycrystalline films. Shown in figure 4b is a similar analysis for BSCCO. The best fit follows power law dependence and U goes as $H^{-0.57}$ in the small external magnetic field up to 2 T and changes to $H^{-0.76}$ at higher fields. This crossover to a slow decay in activation energy at high fields has been

reported in BSCCO 2223 single crystals [18]. Further, the magnitude of U_0 at low fields is an order of magnitude higher in our BSCCO tape platelets as compared to single crystals. The high value of n ($U \sim H^{-n}$) and U_0 in powder in tube processed BSCCO tape is assigned to improved pinning due to granularity, and defects. We note that like BSCCO, in MgB_2 the onset of TAFF behavior occurs at temperature far below T_c . For $NbSe_2$ with equation 2, and $\delta = 2$ the fitting parameter are found to be $a = 631.70$ K, $\gamma = -1.1$, irreversibility field $B^* = 14.45$ T and the parameter of goodness of the fitting $R^2 = 0.98$. It suggests that in $NbSe_2$ U versus H follows the behavior like that for polycrystalline MgB_2 . The low field activation energy for $NbSe_2$ is of the same order as BSCCO. We also note that in the low field region below 2 T, the activation energy is $NbSe_2$ decreases faster as compared to MgB_2 . In intermetallic superconductors, the intergrain pinning is the most dominant flux pinning mechanism because the average grain boundary is far wider than inter vortex distance. The flux pinning force in this regime is given by Kramer's scaling law that is $F_p = J_c \times B = (B/B^*) (1 - B/B^*)^2$ [19,20]. Therefore we conclude that the parabolic field dependence of activation energy as observed in polycrystalline MgB_2 , and $NbSe_2$ is attributable to strong grain boundary pinning.

The TAFF regime, in the presence of anisotropy, thermal fluctuation, and granularity, has been the focus of many studies [7]. The three parameters that define the TAFF behavior are the i) thermal energy kT , ii) correlated vortex-bundle volume (related to anisotropy) and iii) effectiveness of grain boundary pinning (related to coherence length). We note that while the anisotropy of all the three superconductors are comparable [3, 21], there is a vast difference between the coherence length and thermal energy kT . While the large coherence length and the size of the as grown point defects in MgB_2 enables strong grain boundary pinning, the larger anisotropy leads to greater U_0 at low fields. The magnitude of U_0 at low fields is given by $U_0 \sim \phi_0^2 \xi / 48 \pi^2 \lambda^2$ [17]. For MgB_2 using the value $\xi \sim 5$ nm and $\lambda \sim 100$ nm [22] U_0 is estimated to be ~ 10000 K. Similarly for BSCCO using the value $\xi \sim 0.09$ nm and $\lambda \sim 194$ nm [23] U_0 is found

to be ~ 7400 K where as for the case of NbSe₂ with $\xi \sim 2.3$ nm and $\lambda \sim 230$ nm, U_0 is calculated to be ~ 1000 K. This explains our data very well. Thus we find that while the vulnerability to thermal fluctuation is characterized by $1/\xi_{ab}\xi_c$, the magnitude of U_0 at low field goes as ξ/λ^2 .

To gain further insight into the pinning properties of bulk MgB₂, in figure 5 we replot the $\rho - J$ graph of figure 2 with scaling parameters as applicable to vortex glass theory [24]. Our objective is to see whether the vortices in MgB₂ behave as 3 D lines or do they decouple into 2D pancakes as seen in BSCCO superconductors [25]. The VGT predicts a change in curvature for log V versus log I curves at a temperature defined as the vortex glass transition T_g . The exponents for such universal scaling mechanism give information about the dimensionality of vortices on superconducting systems. The scaled I - V curves at H = 3 T show the curvature change at $T_g = 28.8$ K. The fitting parameters are found to be $z = 4.6$ and $\nu = 1.05$. These values correspond to 3D vortices in our MgB₂ samples.

In conclusion, we identify thermally assisted flux flow regime in clean polycrystalline MgB₂. The calculated activation energy for NbSe₂ and MgB₂ follows a parabolic field dependence that is analyzed in the general framework of grain boundary pinning. C-axis oriented BSCCO platelets on the other hand follow a power law dependence $H^{-\eta}$ with $\eta \sim 0.57$ in the low magnetic field up to ~ 1 T. We also find that at low fields the activation energy U_0 relates to the ratio ξ/λ^2 where as its vulnerability to thermal fluctuations is decided by the ratio $1/\xi_{ab}^2\xi_c$.

Acknowledgement

We thank J. Jiang and I. Naik for the BSCCO and NbSe₂ samples and very useful discussions. SBP thanks Department of Science of Technology, India and SDK thanks Council of Scientific and Industrial Research, India for financial support.

References

1. Palstra T T M, Batlogg B, Van Dover R B, Schneemeyer L F and Waszczak J V 1990 Phys. Rev. B 41 6621
2. Nagamatsu J, Nakagawa N, Muranaka T, Zenitani Y and Akimitsu J 2001 Nature 410 63
3. Canfield P C and Crabtree G W 2003 Phys. Today 56 34
4. Gurevich A 2004 Supcond. Sci. Technol. 17 278
5. Grant P 2001 Nature 441 532
6. Masui T, Lee S and Tajima S 2003 Physica C 383 299
7. Blatter G, Feigel'man M V, Geshkenbein V B, Larkin A I and Vinokur V M 1994 Rev. Mod. Phys. 66 1125
8. Pissas M, Lee S, Yamamoto A and Tajima S 2002 Phys. Rev. Lett. 89 097002; Angst M, Puzniak R, Wisniewski A, Jun J, Kazakov S M and Karpinski J 2003 Phys. Rev. B 67 012502
9. Fletcher J D, Carrington A, Diener P, Rodiere P, Brison J P, Prozorov R, Olheiser T and Giannetta R W 2007 Phys. Rev. Lett 98 057003
10. Patnaik S, Gurevich A, Bu S D, Kaushik S D, Choi J, Eom C B and Larbalestier D C 2004 Phys. Rev. B 70 064503
11. Jiang J, Cai X Y, Chandler J G, Rikel M O, Hellstrom E E, Parrella R D, Dingan Yu, Li Q, Rupich M W, Riley G N and Larbalestier D C 2001 IEEE Trans. Appl. Supercond 11 3561
12. Braccini V, Cooley L D, Patnaik S, Larbalestier D C, Manfrinetti P, Palezona, Siri A S 2002 App. Phys. Lett. 81 4577
13. Nato K, Morohashi S, Arfikawa K, and Muto Y 1980 Physica B 99B 204
14. Rowell J M 2003 Supcond. Sci. Technol. 16 R17

15. Qin M J, Wang X L, Soltain S, Li A H, Liu H K, and Dou S X 2001 Phys. Rev. B 64 060505
16. Bardeen J and Stephen M J 1965 Phys. Rev. 140 A 1197
17. Thompson J R, Sorge K D, Cantoni C, Kerchner H R, Christen D K and Paranthaman M 2005 Supercond. Sci. Technol. 18 970
18. Wang X L, Li A H, Yu S, Ooi S, Hirata K, Lin C T, Collings E W, Sumption M D, Bhatia M, Ding S Y and Dou S X 2005 J. Appl. Phys. 97 10B114
19. Cramer E J 1973 J. Appl. Phys 44 1360
20. Cooley Lance, Song Xueyan and Larbalestier David 2003 IEEE Trans Appl. Supercond. 13 3280
21. Ikebe M, Katagiri K, Nato K and Muto Y 1980 Physica 99B 209
22. Thompson J R, Paranthaman M, Christen D K, Sorge K D, Kim H J and Ossandon J G 2001 Supercond. Sci. Technol. 14, L17
23. Li Qiang , Suenaga M, Gohang Junho, Finnemore D K, Hikata T and Sato K 1992 Phys. Rev B 46 3195; Li Qiang, Fukumoto Y, Zhu Y, Suenaga M, Kaneko T, Sato K and Simon Ch. 1996 Phys. Rev B 54, R788; Fossheim K and Sudbø A, Superconductivity: Physics and applications 2004 1st Edition, John Wiley & Sons Ltd, West Sussex p 207
24. Kim Hyeong-Jin, Kang W N, Choi Eun-Mi, Kim Mun-Seog, Kim Kijoon H P and Lee Sung-Ik 2001 Phys. Rev. Lett 87 087002
25. Safar H, Rodriguez E, de le Cruz F, Gammel P L, Schneemeyer L F and Bishop D J 1992 Phys. Rev. B 46 14238

Figure Captions:

Figure 1: Normalized resistivity is plotted against reduced temperature at constant magnetic field for sample under study. Upper layer shows data for MgB₂ at the magnetic field 0, 0.1, 0.25, 0.5, 0.75, 1, 1.5, 2, 3, 4, 5, 6 T. Normalized magneto-resistance for BSCCO at magnetic field 0, 0.1, 0.25, 0.5, 1, 2, 3, 4, 5 T is shown in middle layer. Magneto-resistance for NbSe₂ at magnetic field 0, 0.1, 0.25, 0.5, 0.75, 1, 1.5, 2, 3, 4, 5 and 6 T is shown in lower layer. Inset in each layer depicts zero field resistivity from room temperature to low temperature.

Figure 2: Resistivity is plotted as a function of current density under the influence of external magnetic field of 3 T at constant temperatures.

Figure 3: Resistivity on the log scale is plotted against the inverse of temperature at varying magnetic field for MgB₂, BSCCO and NbSe₂ in respective layers. Arrhenius behavior is observed (see text).

Figure 4: Vortex activation energy U_0 is plotted against the field H for MgB₂, BSCCO and NbSe₂ on log – log scale. Joining lines are curve fitted with the relation mentioned in the figures.

Figure 5: Current density and resistivity behavior has been scaled to test vortex glass behavior. Scaled current density $J_{sc} = J/T(1-T/T_g)^{2\nu}$ is plotted as a function of scaled resistivity $\rho_{sc} = \rho/(1-T/T_g)^{\nu(z-1)}$.

Figure 1

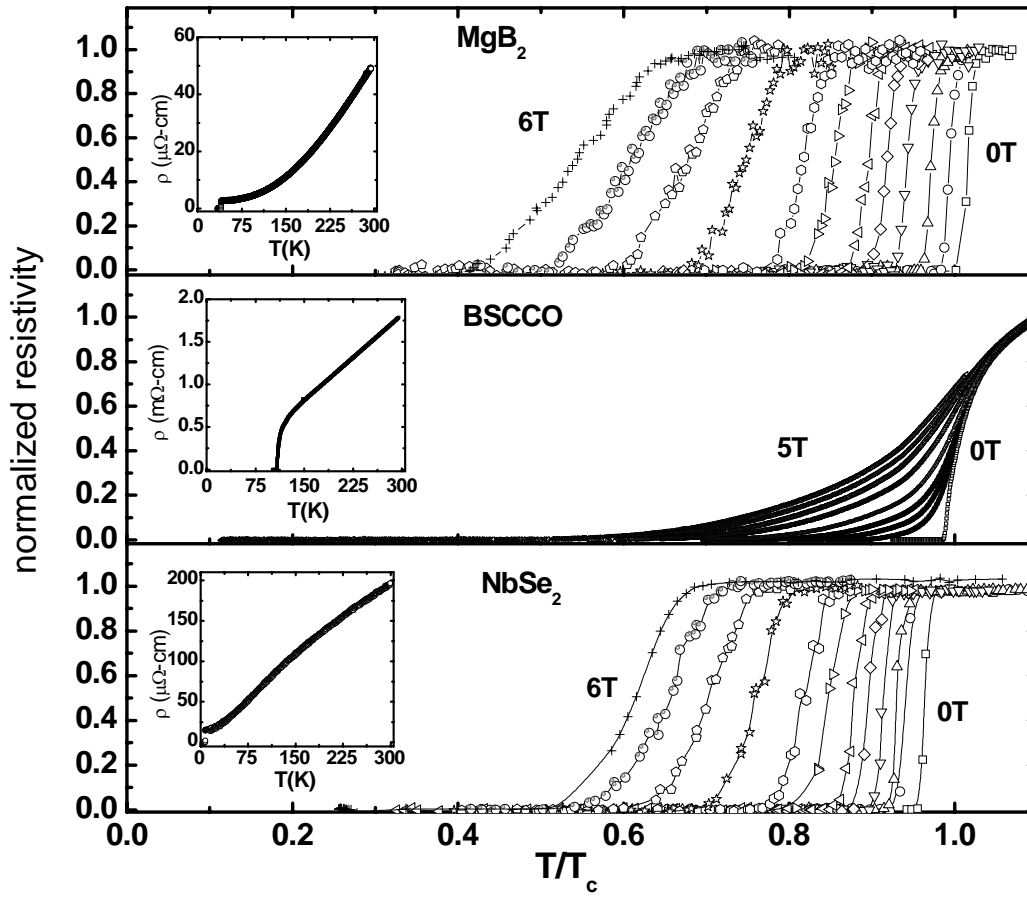


Figure 2

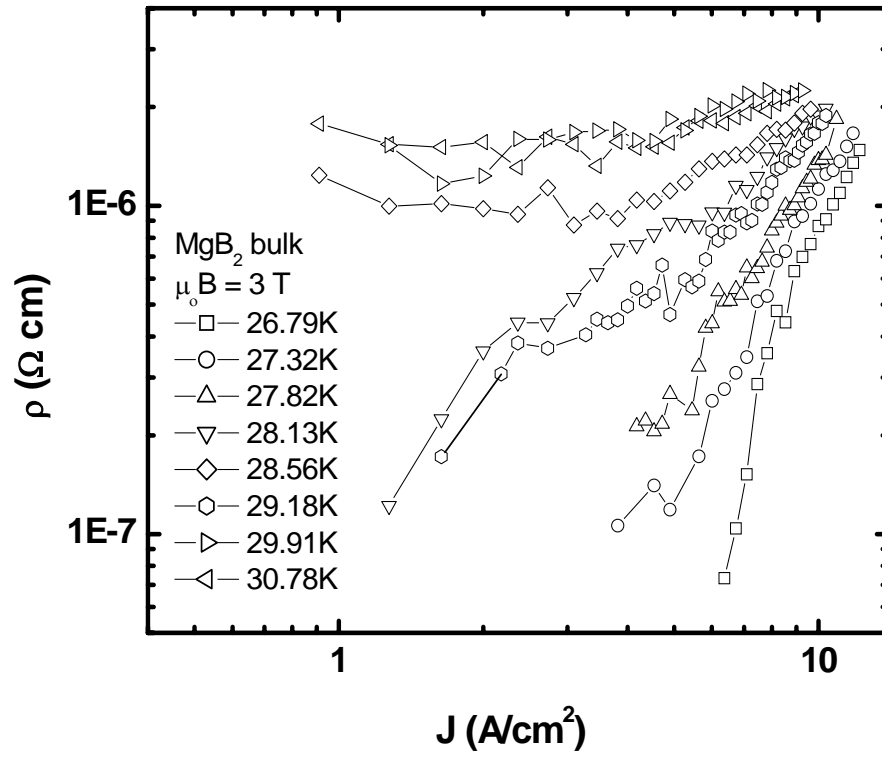


Figure 3

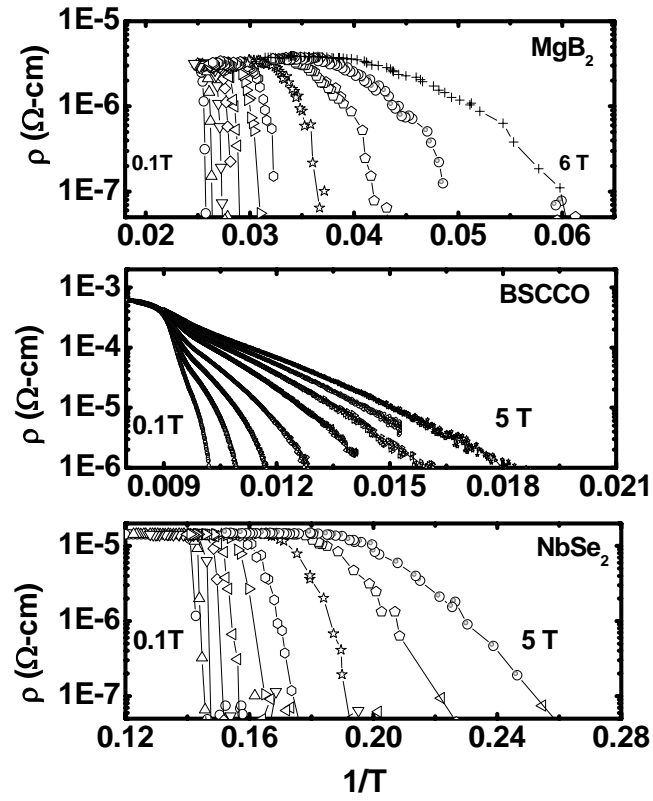


Figure 4

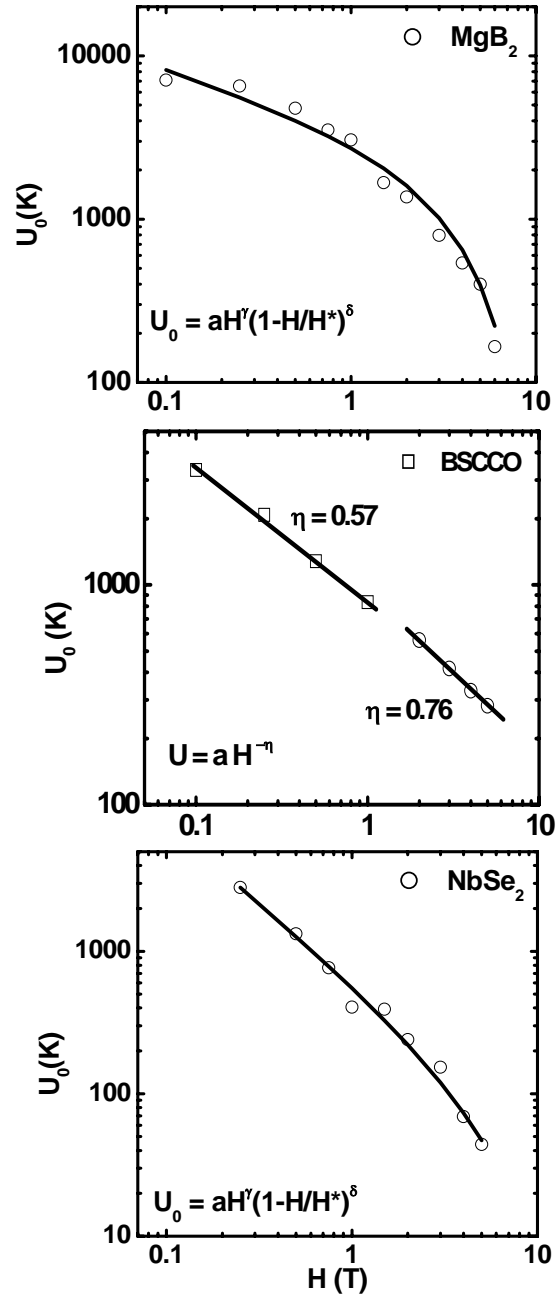


Figure 5

